Soils and Rocks
www.soilsandrocks.com
An International Journal of Geotechnical and Geoenvironmental Engineering
ISSN 1980-9743
ISSN-e 2675-5475

Development of a low cost experimental trigger for dynamic compaction and dynamic replacement

Tennison Freire de Souza Junior[1#], Tiago de Jesus Souza[2], Anderson Bonsanto[3], Gustavo Pizarro Meneghello[4], Tiago Augusto Pianezzer[5]

Case Study

Keywords
Dynamic compaction
Dynamic replacement
Experimental trigger
Finite element analysis

Abstract

Dynamic compaction and dynamic replacement represent techniques for improving soils with low bearing capacity or with a high degree of deformability. Those techniques are performed through the percussive process of large hammers or plates with metric tons of weight released from large heights on the soil. Currently, there are many companies worldwide using different types of equipment with distinct specifications regarding height and lifting capacity, potency and release form (cables or free fall). For experimental purposes, this article proposes the development of a trigger system composed of a release lever and a body, which is formed by the fixed body, the moving body and a lock, inspired by Giese (2019). The proposed trigger body was developed with SAE 4140 steel and SAE 1020 steel in connection with the low cost release body. After the tests, the objective of the study was achieved in the laboratory tests (80 kN) and field tests (55 kN of tamper weight plus friction and adherence between soil/tamper).

1. Introduction

Soil improvement or reinforcement involves the modification or manipulation of physical and chemical processes to enhance the mechanical properties and parameters of soil, such as shear strength, compressibility, and hydraulic conductivity, in order to meet specific requirements in civil construction projects. In recent years, various innovations in geotechnical engineering have explored commercial solutions for improving and reinforcing different soil types. These include consolidation methods (e.g., vertical drains and vacuum consolidation) and reinforcement techniques with driven aggregate piles, controlled modulus columns, dynamic replacement, jet grouting, and vibro-replacement (Kézdi, 1979); Geosyntethics (Koerner, 1997); Chemical methods with Portland cement, Lime and Betuminous (Ingles & Metcalf, 1973); as well as compaction methods with vibro-compaction and dynamic compaction (Slocombe, 2013; Hamidi, 2014; Giese, 2019). Concepts and other soil improvement methods can be found in the works of Mitchell (1981), Terashi & Juran (2000), Han (2015) and Almeida et al. (2022).

Dynamic compaction can lead to significant soil improvement at substantial depth, often with considerable savings when compared to other geotechnical solutions (Hamidi, 2014). It has become a popular method for deep improvement of soils, especially in Middle Eastern, European and North American countries. According to Souza Júnior (2021), dynamic compaction has existed since Roman times in a rudimentary form, without standardized technical procedures. Formally, dynamic compaction was standardized through large-area improvement techniques developed by Menard, as presented in Menard (1974) and Menard & Broise (1975), using adapted machinery.

The method involves repeated application of high energy impacts on the soil surface using compactors with 20 t of weight, falling from 20 m high, for densification or consolidation the soil layer to a considerable depth (Slocombe,

#Corresponding author. E-mail address: tennisonufpr@outlook.com
[1]Universidade Federal do Paraná, Departamento de Engenharia Civil, Curitiba, PR, Brasil.
[2]Universidade Federal de São Carlos, Departamento de Engenharia Civil, São Carlos, SP, Brasil.
[3]Universidade de La Salle, Departamento de Engenharia Mecânica, Porto Alegre, RS, Brasil.
[4]Universidade Federal do Rio Grande do Sul, Departamento de Engenharia Mecânica, Porto Alegre, RS, Brasil.
[5]Universidade Federal de Santa Catarina, Departamento de Engenharia Civil, Florianópolis, SC, Brasil.

Submitted on November 27, 2024; Final Acceptance on February 27, 2025; Discussion open until August 31, 2025.
Editor: Renato P. Cunha https://orcid.org/0000-0002-2264-9711
https://doi.org/10.28927/SR.2025.008324

2013; Pan & Selby, 2002). The specifications of the compaction weights, heights and distance between compaction points are defined as a function of the improvement to be achieved, based on the design needs. Therefore, these parameters vary according to the soil improvement depth. There are reports of different studies using varied compaction weights and fall heights, such as those presented by Slocombe (2013), Pan & Selby (2002), Gambin (1983), Mayne et al. (1984), Rollins & Rogers (1994), Feng et al. (2011), Hamidi (2014).

Currently, there are many companies worldwide that work with this type of technique on different types of soil. In these companies, there are several pieces of equipment with different configurations and specifications, such as shape, lifting height, lifting capacity and release form (free fall or through cables) (Hamidi, 2014). However, although there are commercial trigger systems available, there are few reports of this device in the literature. For experimental purposes, a method was released at Federal University of Rio Grande do Sul (UFRGS) to drop compaction hammers with the aid of cranes, simplified trigger, straps and bundles of steel cable in order to investigate the effect of compaction on Brazilian tropical soils (Giese, 2019; Rizzon, 2016). Based on the experiences of previous studies (Giese, 2019; Rizzon, 2016), this paper aims to present the development of an experimental manual release trigger designed for low-cost dynamic compaction and dynamic replacement coupled to a crane system.

2. Dynamic compaction and dynamic replacement method

2.1 Principle of technique

Dynamic compaction method involves the repeated application of high energy impacts on the soil's surface using either concrete or steel compactors weighing 100-250 kN, falling from heights of 10 m to 30 m high, compressing the soil strata to a considerable depth. These weights, also known as hammers, are released repeatedly on the same impact spot according to a predetermined standard (Porán & Rodriguez, 1992). The mass and the fall height of the compactor vary according to each researcher; however, the order of magnitude remains the same (e.g., Slocombe, 2013; Mayne et al., 1984; Feng et al., 2011; Hamidi, 2014; Menard & Broise, 1975; Craig, 2012; Feng et al., 2015). Additionally, the number of hits varies according to the type of soil and as a function of the dissipation of the water pressure (Menard & Broise, 1975).

The principle of the technique is based on the reduction of intergranular empties, specifically for treatment of natural, mixed and cohesive sands (Giese, 2019). However, the technique was extended to fine soils (silts and clays), where high energy impact effectively provides a concentrated load that dissipates water pressure from silts and clays, known as dynamic consolidation (Menard & Broise, 1975). Dynamic replacement was then developed to build large-diameter columns of granular materials through soft grounds close to the surface, particularly for turf and Sabkha layers (Hamidi, 2014; Tarawneh et al., 2017; Tarawneh et al., 2019).

As dynamic replacement represents a specialized form of compaction, there are many similarities between both processes, such as hammer mass, fall height and equipment. In this method, the granular fill is dynamically compressed through a percussive process involving loads varying from 150 kN to 250 kN and heights from 10 m to 25 m (Tarawneh et al., 2017). It produces a large diameter reinforced soil column (known technically as pillar) with diameters from 2.0 m to 2.5 m and depths of up to 7 m. On average, this method might reach replacement rates of up to 25% and each column has a load capacity up to 1500 kN.

2.2 Items and equipment

Regarding equipment specifications, in Onshore constructions it is used wheeled or crawler cranes to lift hammers from 15 t to 25 t. The Menard Tripod can also lift hammers up to 40 t (Hamidi, 2014). Hammers are typically built from hardened steel sheets, box steel and concrete or concrete of suitably reinforced mass and distinct geometries, where durability is the main requirement. From a technical point of view, the geometry and the contact tension of the base are relevant aspects to the formation of craters (Giese, 2019; Mayne et al., 1984; Rizzon, 2016; Mehdipour & Hamidi, 2017), to the influence depths (Mayne et al., 1984; Smits & De Quelerij, 1989; Lukas, 1995; Ghassemi et al., 2009; Hajialilue-Bonab & Rezaei, 2009) and affecting the plasticizing bulbs (Porán & Rodriguez, 1992; Oshima & Takada, 1997). In terms of release methods, the literature reports that hammers can be released by free falls or cables.

In the free fall method, the hammer is released without cables from a specified height, reducing friction losses. In contrast, for the cables system, the hammer is released while fixed to steel cables in a similar way to that which occurs to pile drivers. Ménard has developed a trigger system that enables a pseudo free fall, on which the hammer is released in free fall with a cable fixed on the trigger in order to prevent the impacts between the hook and the boom, called MARS (Menard Accelerated Release System) (Hamidi, 2014).

Giese (2019) has developed a trigger with a manual aperture system, similar to the MARS one. The device was produced with SAE 1020 steel, which is simple carbon, with other negligible elements in percentage and manganese content of 1%, and flow resistance value of 351,6 MPa. However, the trigger created presented: reduced lever stroke; lock/lever connection limited to the cable and therefore low stiffness which gave fatigue of the connection; body steel with stiffness and strength not corresponding to lifting forces; and no steel protecting system.

The cost of acquisition and maintenance is extremely high, which makes the method often not economically feasible. The proposed trigger coupled to a crane can be an interesting alternative for soil improvement in works of low to medium complexity due to the proven efficiency of the method in soil treatment. Another important point to be exposed is the sustainability generated by the method of dynamic compaction and dynamic replacement because the method is free of the use of cementing agents and allows the use of demolition waste as fill material.

3. Trigger conception

3.1 Dispositive function

The operation of the trigger is based on the principle of moments. Once the hammer is lifted to the designed height, it is released by lifting the lock fixed on the release lever, which prevents the moving body from tipping prematurely. The tipping of the moving body allows the handle, attached to the hammer, to be released into free fall. This moment is produced by a force at the end of the lever, which is derived from the tensile force on the wire attached to its end (Figure 1). This wire is designed to disengage the hammer at the desired height. The effort to release the wire is carried out manually by the operator.

3.2 Trigger details

The software Autocad® (student Version) was used to detail the views of the device created for simulation and machining of the parts. It is shown in Figure 2 the dimensions of the complete body and of the moving body and in Figure 3 the detailed dimensions of the fixed body. Finally, Figure 4 shows the detailed dimensions of the lock and its opening system. Cuts and geometric details of the piece can be seen in more detail in Souza Júnior (2021).

4. Materials and methods

In terms of loading on the trigger, it was considered a load of 70 kN. This corresponds to the static effort to remove the hammer from the crater, which is the sum of the load of the weight of the compaction hammer, the base adhesion of the it and the friction of its base. For this, the trigger was modeled with the cylinder coupling supported in a delimited region of the moving body (as it simulates the handle supported in the part) based on Finite Elements Methods (FEM).

The trigger body was designed with SAE 4140 steel, which is a chromium-molybdenum alloy characterized by high mechanical strength, stiffness and fatigue, impact and abrasion resistance. The release lever of the hammer was

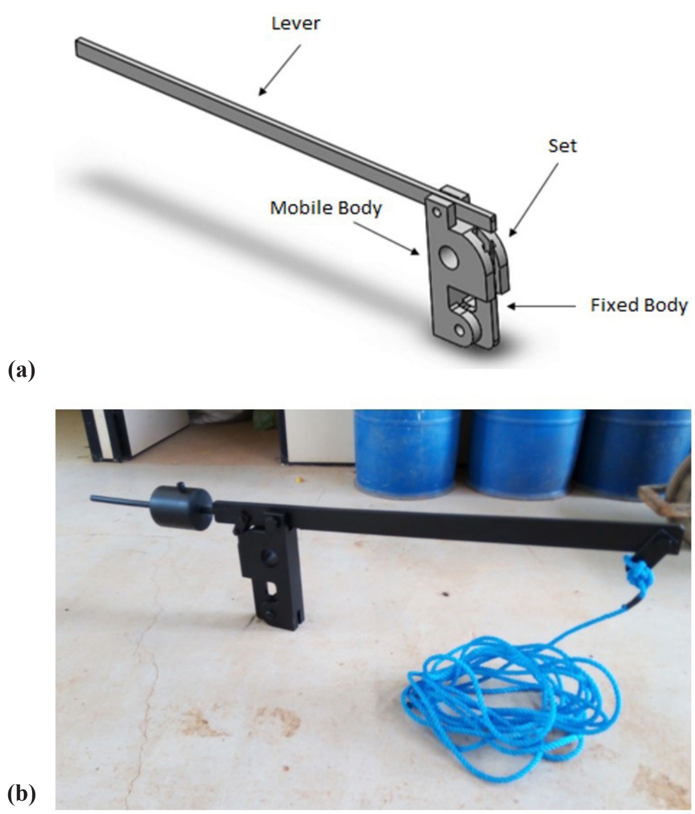

Figure 1. Experimental trigger: (a) 3D-Figure in Solidworks®; (b) built.

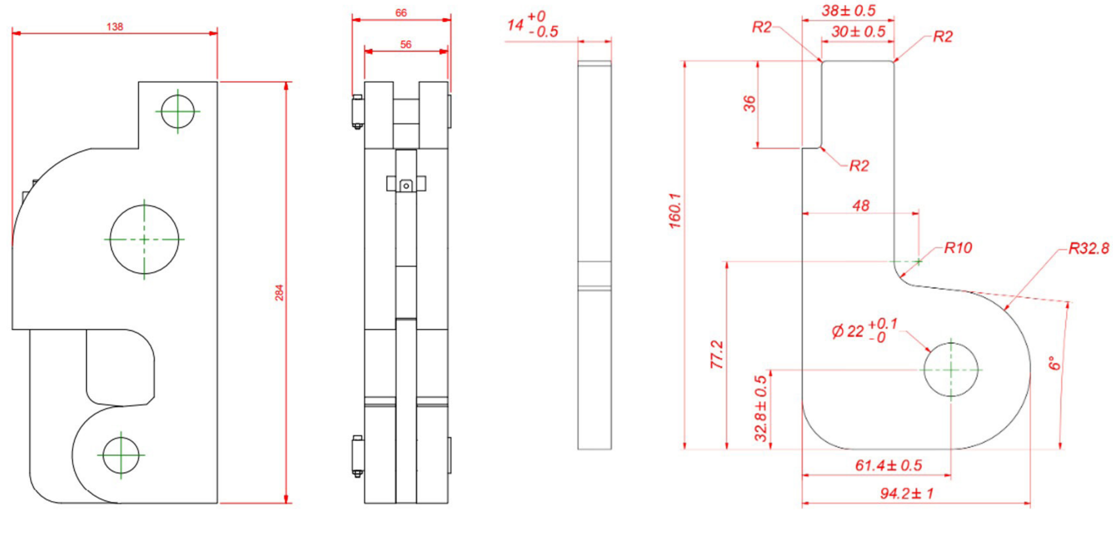

Figure 2. Details of the complete body and the moving body (in millimeters): (a) side view of the complete body; (b) front view of the complete body; (c) front view of the moving body; (d) side view of the moving body.

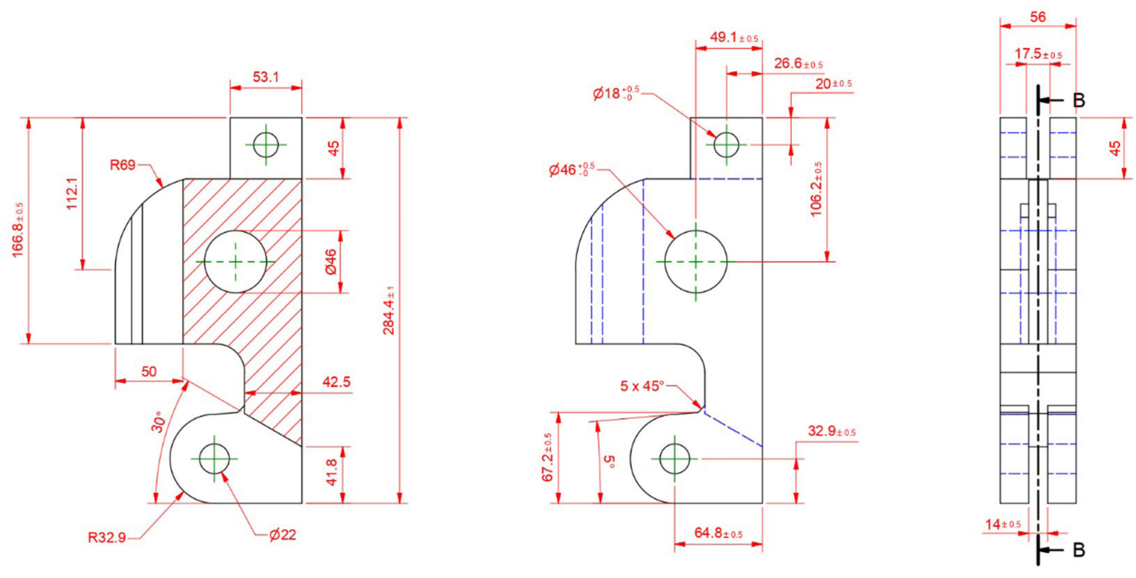

Figure 3. Details of fixed body (in millimeters): (a) side section of fixed body – section B-B; (b) side section of fixed body; (c) front view of fixed body.

designed with SAE 1220 steel, which is a carbon steel consisting basically of iron, carbon, silicon and manganese. It has lower mechanical properties compared to SAE 4140 steel, as it will not be subjected to high stress. The chemical compositions of both materials are described in Table 1, according to ABNT (2000), and the mechanical properties are described in Table 2.

The trigger was designed with Solidworks® Software, version 2016. It was based on FME using a mixed standard mesh with 4 Jacobian points and it was also performed a mesh convergency test based on 5 evaluations. Von Misses' plastic constitutive model is suitable for the description of the behavior of ductile materials such as metals (Chen & Han, 1988). This model, according to Chen & Han (1988) and Chen & Zhang (1991) is based on the following premises:

a. Von Mises' criteria states that the plasticization of a material would occur when the maximum shear strain energy at a point in the material reaches a

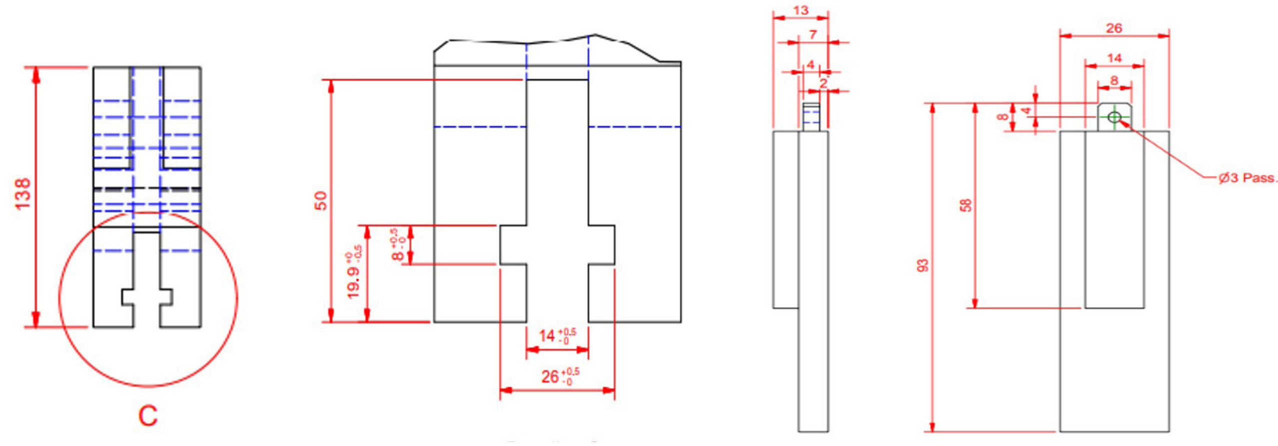

(a) (b) (c) (d)

Figure 4. Details of the lock (in millimeters): (a) upper view; (b) dimensions of upper view; (c) side view of lock opening system; (d) lock front view.

Table 1. Chemical composition of steels used in the trigger (ABNT, 2000).

Steel	C (%)	Mn (%)	Si (%)	Cr (%)	Mo (%)	P (%)	S (%)
SAE 1020	0.18 – 0.23	0.30 – 0.60	---	---	---	0.040 (max)	0.050 (max)
SAE 4140	0.38 – 0.43	0.75 – 1.00	0.15-0.35	0.80-1.10	0.15-0.25	---	---

Table 2. Mechanical properties of the steel used on the trigger design.

Properties	Unity	Steel	
		SAE 4140	SAE 1020
Modulus of Elasticity	GPa	209.00	211.00
Poisson Coefficient	---	0.32	0.29
Shear Modulus	GPa	81.57	77.00
Specific Mass	kg/m^3	7850.00	7900.00
Tensile Strength	MPa	1132.00	420.00
Yield Value	MPa	724.00	351.57

critical value, this energy being proportional to the second variant of the stress tensor;

b. An associated flow rule assumption is made, where the plastic flow is associated with the yield criterion;
c. Isotropic and kinematic hardening rules are valid, as the associated flow rule for irreversible plastic materials is applicable, meaning plastic deformation cannot be recovered;
d. In large plastic flow problems, elastic tension can be neglected, and the material can be idealized as rigid and perfectly plastic.

To certify the quality of SAE 4140 steel of the trigger body, 10 samples were tested, being 5 tensile tests, following the procedures of ABNT (2015), and 5 Charpy impact tests, following ASTM E-23 specifications (ASTM, 2018), as shown in Figure 5. In addition, 5 hardness tests were performed on an impact strength sample (see CP5 in Figure 5), based on ABNT (2009) and ASTM (2019).

Figure 6 shows the equipment used to certify the quality of the steel used in the composition of the trigger body. As can be seen in Figure 6a, the electronic press used in the direct tensile tests was the model AGX Plus, with capacity up to 250 kN, of the company Shimadzu®. Figure 6b shows the Charpy test equipment, with a hammer of 30 kpm (with a mass of 18,75 kg and a rotating arm length of 0.825 m), made by German company Wekstoffprüfmaschinen Leipzig®. Finally, Figure 6c presents the Digital Hardness Test, model Duravision 30, from the company EMCO TEST®, with Rockwell C test option of 150 kgf load.

A tensile test was performed in the laboratory to validate and verify that the trigger modeled in software Solidworks®, version 2017, was consistent with the mechanical forces expected in the field. In addition, a Strain Gage model PA 09 060TG 350L (see Figure 7) was used to monitor the behavior of the trigger fixed body.

In the automated press, illustrated in Figure 6a, the trigger was attached to two handles, each of which was held

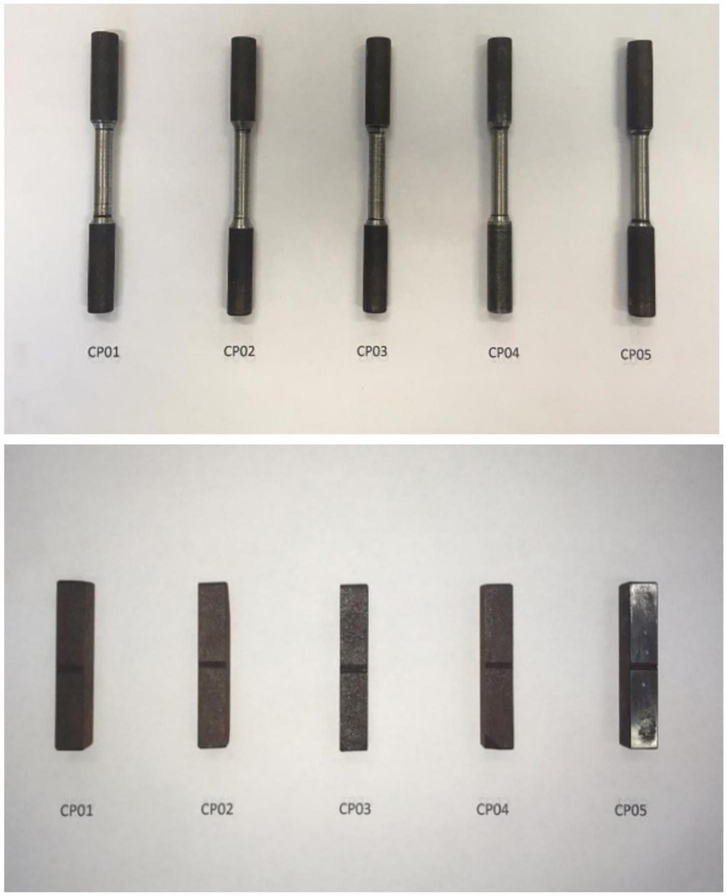

(a)

(b)

Figure 5. SAE 4140 steel sample: (a) direct tensile tests sample; (b) impact tests sample.

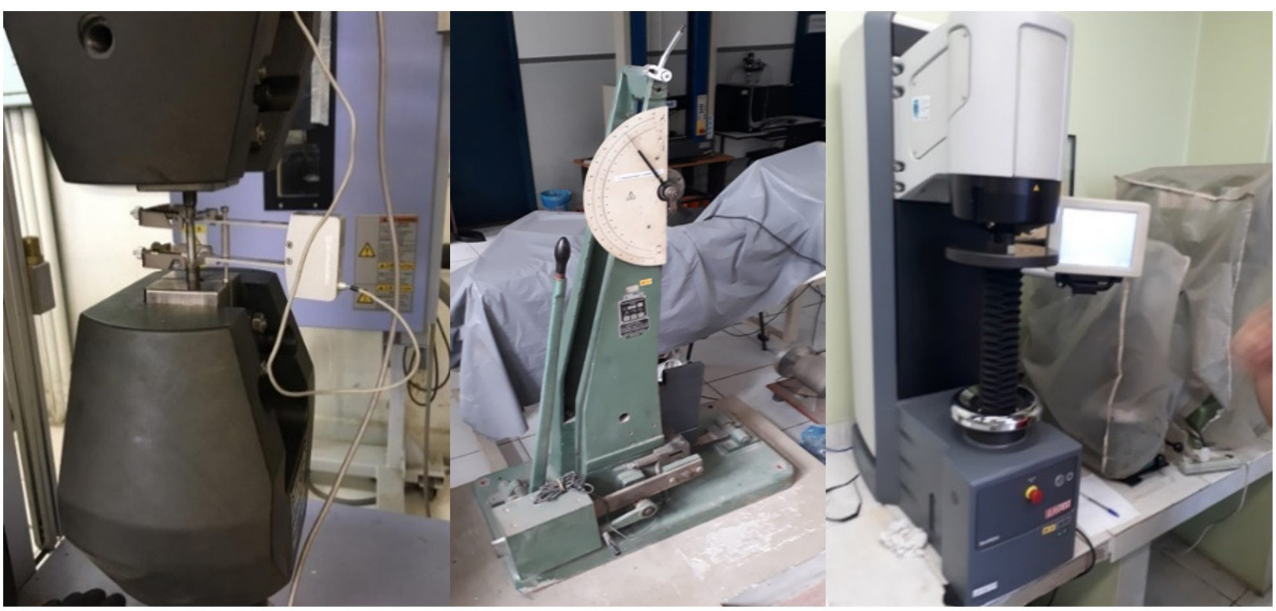

(a) (b) (c)

Figure 6. Equipment used for steel testing: (a) electronic press for direct tensile test; (b) impact test equipment; (c) hardness test equipment.

by a steel rope loop, which were fixed to the press claws, as shown in Figure 8. Deformation measurements were evaluated during the application of the monotonic load, through a strain gauge, as shown in Figure 9. It was attached to the face of the fixed body with highest stress, according to the numerical modelling.

(a)

(b)

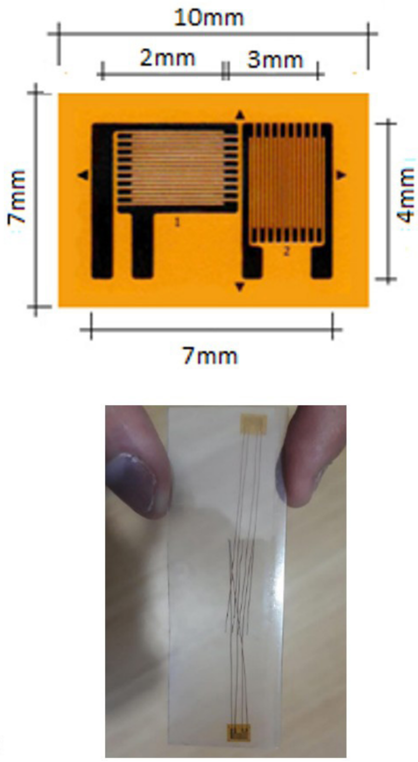

Figure 7. Strain gage model PA 09 060TG 350 L: (a) detail schematic; (b) real illustration.

The static equilibrium was used, with Ftool® Software, to determine the trigger lever length. For this, three analytical simulations were performed, with lengths of 0.4 m, 0.6 m and 0.8 m, and a fixed support was created at the end of the lever drive to release the lock. Hypothetically, the fixed support reaction would be achieved with the minimal effort to keep the system in balance. Therefore, if a higher load were applied to the fixed support, the static system would be transformed into a mechanism.

5. Results and discussions

The numerical convergence test of the mesh on the trigger showed that using a 0.007 m mesh on the body as well as refining the mesh in the support region with a 0.005 m characteristic size element, was sufficient for a consistent simulation, since the impact on its results was less than 1%, as shown in Table 3.

Numerical analysis was performed by adopting the scenario with characteristic size of the element with 0.005 m in the trigger body and 0.002 m in the region with the

Table 3. Numerical convergence test of the mesh on the trigger.

Characteristic Size of the Element (m)		δ_{max} (mm)
Trigger Body	Mesh Support Region	
0.014	---	0.0461
0.014	0.007	0.0466
0.007	0.005	0.0473
0.005	0.003	0.0475
0.005	0.002	0.0476

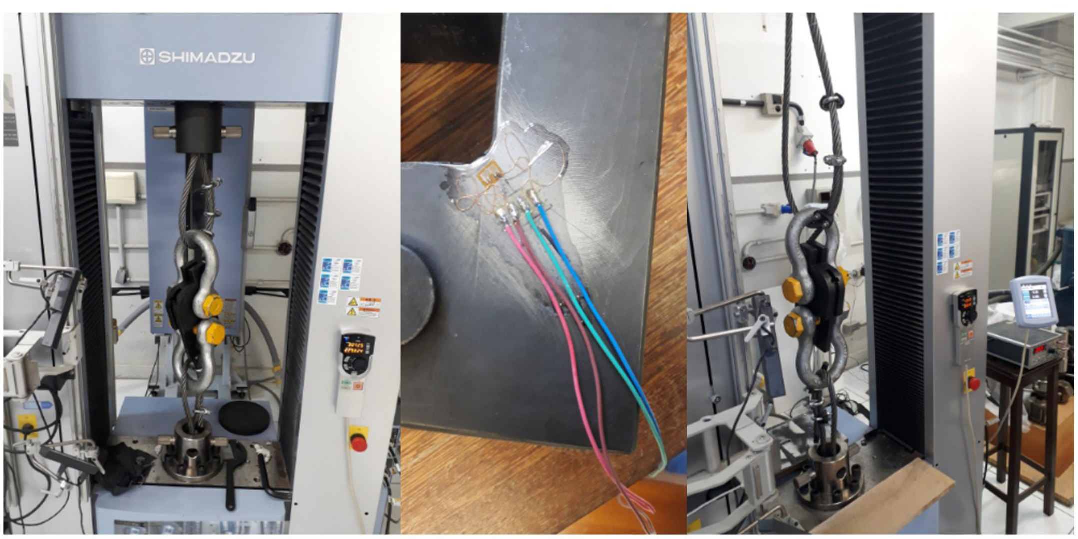

(a) (b) (c)

Figure 8. Direct tensile test: (a) trigger body fixed to the press; (b) strain gauge installation on trigger body; c) test set for trigger deflection reading.

highest stress concentration. Regarding the evaluation of tension and deformation in the elastic system of the trigger body (fixed body with the moving body locked), the numerical simulation showed that the fixed body presented small deformations (maximum of 0.154%) and a maximum stress of 370.11 MPa concentrated in the boundary region between the moving body and the fixed body.

It occurs due to the eccentricity of the lifting hole (top opening) and the coupling point of the weight (support region of the handle with the compaction hammer). The balanced position of the loaded trigger is represented by a slight rotation in the direction of opening the moving body, concentrating high stress in this region. Such eccentricity allows the weight to be released more easily when the device is opened.

Furthermore, in numerical simulation, a maximum displacement of 0.0476 mm was obtained, however, in the other parts of the body, displacements varied from 0.0198 mm to 0.357 mm, as shown in Figure 9a. The standard ASME BTH-1 (ASME, 2008) was used to determine the design factor. According to ASME BTH-1, situations in which the magnitude and load variations are not predicted, or the conditions are classified as severe or not precisely defined, the Category B is then used. In such category, the lifting devices shall not be less than 3.00, for yield or flash limit states, or less than 3.60, for fracture limit states or for connection design.

A value of 1.917 was obtained for the safety factor (FS) of the device. Since the concentrations that caused the reduction of the FS_{min} were punctual, it can be considered that the overall design safety factor of the piece was equal to 3.938, as shown in Figure 9b.

5.1 Trigger steel verification tests

After the tests on the SAE 4140 steel sample, it was perceived, through the results shown in Table 4, that the material is adequate when compared to the input data of the computational simulation, even reaching values higher than the specific one.

Furthermore, as it can be seen in Figure 10, the steel yield value has reached value from 1200 MPa to 1400 MPa, being approximately 65% a 93% bigger than the one used in the trigger modelling. This increase is due to the heat treatment

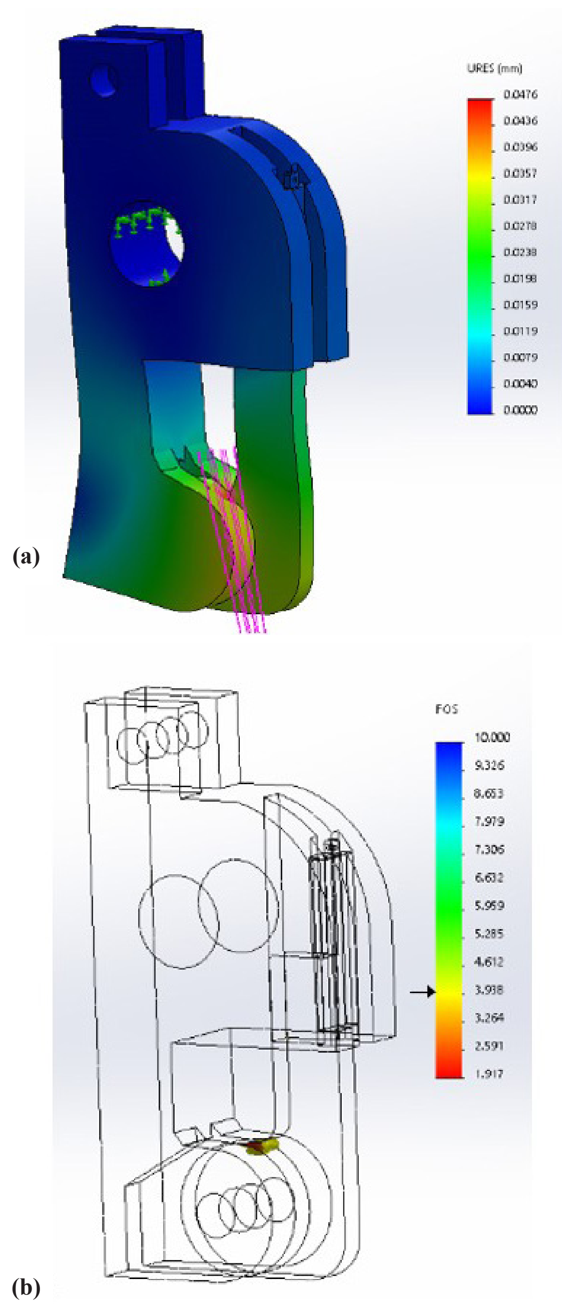

Figure 9. Trigger numerical simulation: (a) evaluation of displacements; (b) evaluation of safety factor.

Table 4. Results of the tests on the SAE 4140 steel sample.

Test	Values					
	1	2	3	4	5	Average
Hardness (HRC)	45.60	45.48	47.05	48.72	45.02	46.37
Impact Resistance (J/Rad)	29.42	29.42	33.34	23.54	32.36	29.62
Tensile Strength at Break (MPa)	1312.37	1337.98	1302.11	1319.34	1327.85	1319.93
Maximum Tensile Strength (MPa)	1402.87	1425.27	1372.69	1402.15	1414.93	1403.58
Yield Value (MPa)	1220.35	1249.99	1247.59	1189.49	1238.19	1225.92
Young's Modulus (GPa)	220.00	229.36	224.26	236.17	230.90	228.14

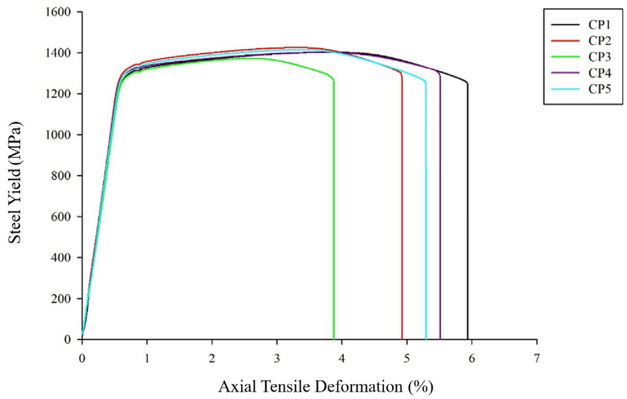

Figure 10. Direct tensile strength tests of SAE 4140 steel sample.

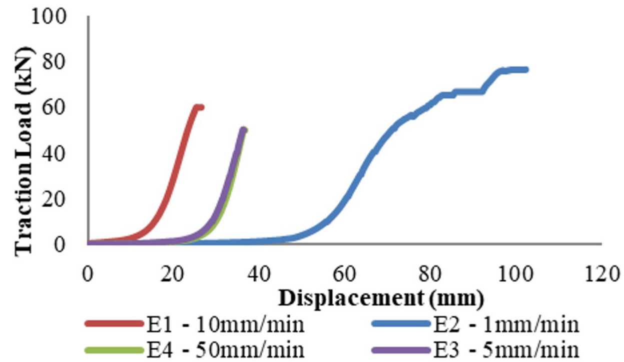

Figure 11. Direct tensile tests of the trigger with the handles attached.

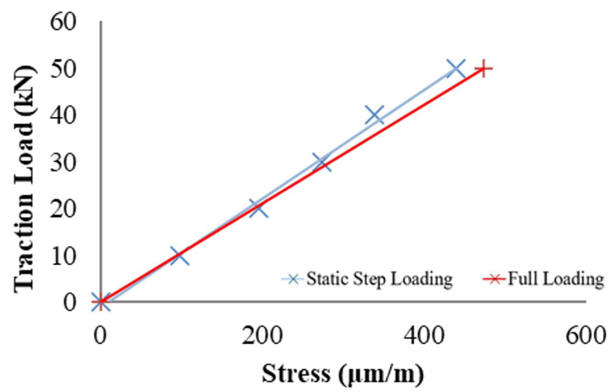

Figure 12. Elastic deformations suffered by the trigger in static step loading (blue) and full loading (red).

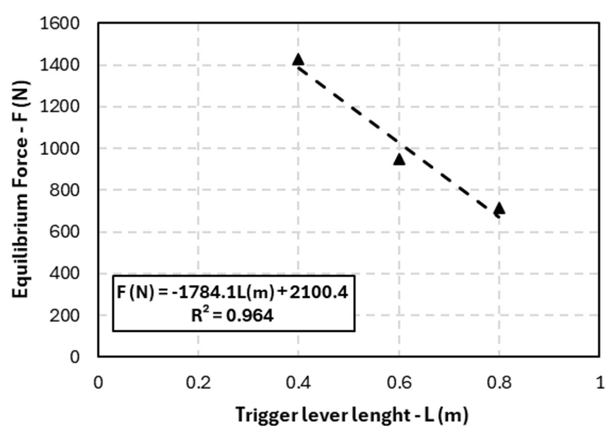

Figure 13. The relationship between lever balance effort and lever length.

process applied to the steel called tempering. The heating and sudden cooling cycle allows better crystal arrangement, that raises the hardness and mechanical strength of the material.

5.2 Trigger verification tests

After the direct tensile tests on the trigger, it was found that the device body, in four tests, performed resisted tensile forces of up to 80 kN (8 t) without damage to the part, although the set has reached large displacements (between 0.020 m and 0.100 m), as shown in Figure 11, due to the stretching effect of the traction cables anchored in the press grip. Unfortunately, it was not possible to create a rigid connection at the time of testing, because there was no device that could easily connect to the trigger.

In terms of deformations suffered by the trigger after static press loading, two tests were performed. The first one was per phase, where every 1 t was stopped and the deformation value was taken, and the second one was per total load, where the deformation value was taken when the load was up to 5 t at the end of the test. By these means, the deformation of the piece was similar. In the first test, the final deformation was equal to 439 μm/m and in the second test it was equal to 474 μm/m. This confirms that the component operates within the elastic regime under the stress/strain levels analyzed, as shown in Figure 12.

5.3. Estimated Selection Length

The verification of the trigger opening force was carried out through simulations using a hyperstatic portic with Ftool® Software. In this model, two loads were applied: one corresponding to the trigger counterbalance (70 N) and the other to the horizontal force component of the hammer's weight (8.437 kN). Variations in the device's lever length were studied at 0.40 m, 0.60 m, and 0.80 m.

As it can be seen in Figure 13, as the lever length increases, the support reaction reduces. This indicates that increasing the lever length reduces the effort required by the operator for locking. While the support reaction value represents a balance effort, slight variations in the effort applied during release—ranging from approximately 10% to 20% — would be sufficient to unlock the trigger from an empirical standpoint. The relation can be considered normalized due to the excellent correlation obtained (R^2=0.964).

It is observed that, with a length of 0.8 m, equivalent efforts of 700 N (corresponding to the average weight of an operator) are achieved, thus reaching what could be considered the minimum length. However, due to the simplicity of the force equilibrium model, a 25% increase was applied, resulting in a total length of 1.0 m.

5.4 Trigger opening tests

The tests were carried out on a 55 kN hammer. In this test, the compaction hammer was hoisted up to 3 m, 5 m and 8 m and, thus, the release of the trigger was evaluated, as can be seen in Figure 14. This evaluation was conducted from a qualitative perspective, aiming to confirm whether the calculated strengths for device opening were consistent. A 70-t capacity crane was employed. To attach the trigger to the crane, a 10-t polyester strap was used coupled to the 20-t shackle. As for the hammer, steel ropes with a loop were used, which were attached to a washer and which, in turn, formed the compaction hammer assembly, according to item 3.1.

A priori, trigger counterbalancing was performed with the use of washers, totaling a mass of 7 kg, and the connection between the lock and the lever with the use of a 0.004 m steel cable. After the trigger opening test, some modifications were made to the structure. First, the washers were replaced by a single weight in the section of the cylindrical axis, because they change their positions when triggered. In addition, the steel cable has been replaced by a 0.008 mm braided multi-stranded rope to facilitate the drive. Finally, the connection between the latch and the lever suffered continuous disruption during the trigger drive, and, therefore, it was replaced by an articulated plate system (latch-lever), according to Figure 15a. Figure 15b presents the details of the modification that occurred in the trigger structure.

6. Conclusion

The present article presented the development of a low-cost experimental trigger device for releasing hammers in dynamic compaction and dynamic replacement methods. The study employed numerical simulations using FEM, applying the Von Mises constitutive model through SolidWorks software. Additionally, laboratory tests were

Figure 14. Field opening verification test.

(a)

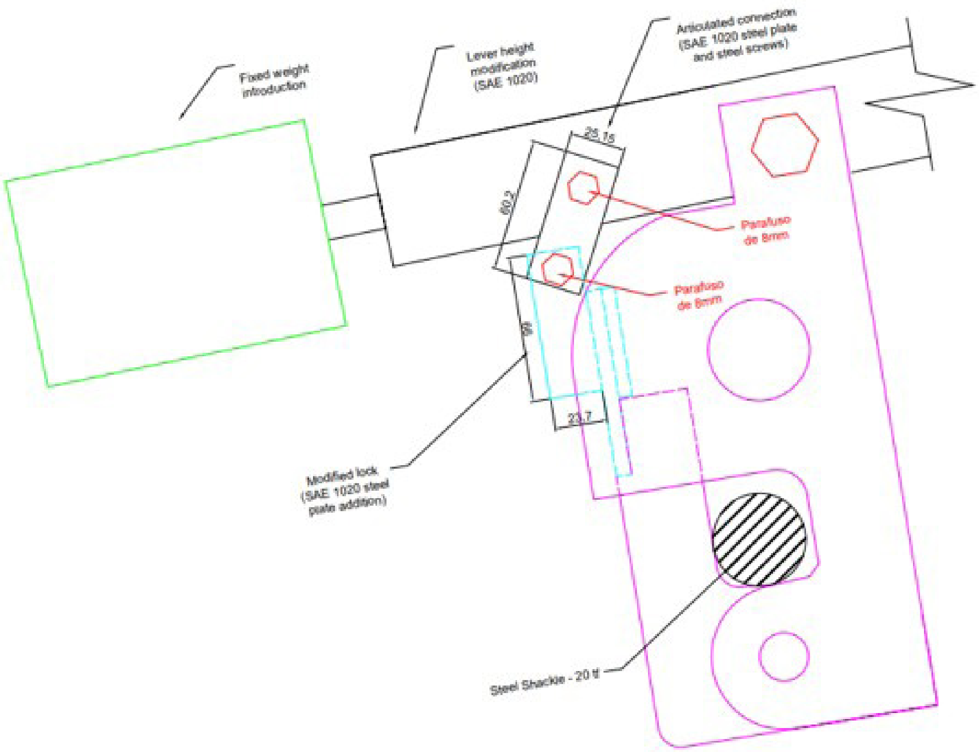

(b)

Figure 15. Modified release trigger: (a) trigger side view; (b) details of the modifications made.

conducted to characterize the material used in the trigger, as well as numerical simulations under monotonic static loading, analyzing the respective mechanical responses of the developed system. Based on the results obtained, the following considerations can be made:

a. As perceived, a value of 1.1917 was obtained when performing the calculation of the safety factor of the piece (FS_{min}). Considering that the concentration that caused the reductions was punctual, it can be considered that, in a general way, the design safety factor of the part was equal to 3.938;
b. As for the evaluation, after the numerical simulation, of the tension by the deformation, in elastic regime, of the trigger body (fixed body with the moving body locked), it was noticed that the fixed body presented small deformations (maximum of 0.154%) and maximum stress of 370.11 MPa concentrated in the boundary region between the moving and the fixed body.
c. In the numerical simulation, a maximum displacement of 0.0476 mm was obtained, however, in the body, the displacements varied from 0.0198 mm to 0.357 mm;
d. Although simplified, the use of isostatic and hyperstatic frames can be interesting alternatives for estimating the length of the trigger lever. Assuming that the support effort created (representing the trigger point) would be the minimum effort to maintain the static system, slightly higher efforts would unlock the mechanism to release the hammer;
e. Field tests have proven that the lever length of 0.8 m is sufficient for the operator to drive and that the designed trigger supports the stresses by the dynamic compaction procedure;
f. As a proposal for future studies, it is recommended to conduct comparative analyses between the proposed device and commercial devices, as well as studies on the dynamic unloading of the device in situations of rapid stress relief.

Acknowledgements

The authors thank CAPES (Coordination for the Improvement of Higher Education Personnel) for the research funding of the PPGEC (Civil Engineering Postgraduate Program) of UFRGS (Federal University of Rio Grande do Sul). Writers would also like to thank anonymous reviewers for their insightful comments and suggestions that have improved the content of this article.

Declaration of interest

The authors have no conflicts of interest to declare. All co-authors have observed and affirmed the contents of the paper and there is no financial interest to report.

Authors' contributions

Tennison Freire de Souza Junior: Conceptualization, Investigation, Methodology, Formal Analysis. Tiago de Jesus Souza: Methodology, Data curation, Writing – original draft, review & editing. Gustavo Pizarro Meneghello: Writing – review. Tiago Augusto Pianezzer: Translation. Anderson Bonsanto: Writing – reviewing & editing.

Data availability

All data produced or examined in the course of the current study are included in this article.

Declaration of use of generative artificial intelligence

This work was not prepared with the assistance of Generative Artificial Intelligence (GenAI).

List of symbols and abbreviations

C	Carbon
Cr	Chrome
FS_{min}	Minimum safety factor
L	Trigger lever length
FEM	Finit Element Method
MARS	Menard Accelerated Release System
Mn	Manganese
Mo	Molybdenum
P	Phosphorus
S	Sulfur
Si	Silicon
UFRGS	Federal University of Rio Grande do Sul
δ_{max}	Maximum stress

References

ABNT NBR NM 87. (2000). *Aço carbono e ligados para construção mecânica: designação e composição química*. ABNT - Associação Brasileira de Normas Técnicas, Rio de Janeiro, RJ (in Portuguese).

ABNT NBR NM ISO 6508-1. (2009). *Materiais metálicos: escala de dureza rockwell – parte I: método de ensaio (escalas: A, B, C, D, F, G, H, K, N, T)*. ABNT - Associação Brasileira de Normas Técnicas, Rio de Janeiro, RJ (in Portuguese).

ABNT NBR 6892. (2015). *Materiais metálicos – ensaio de tração - parte 1: método de ensaio à temperatura ambiente*. ABNT - Associação Brasileira de Normas Técnicas, Rio de Janeiro, RJ (in Portuguese).

Almeida, M.S.S., Marques, M.E.S., Riccio, M., Fagundes, D.F., Lima, B.T., Polido, U.F., Cirone, A., & Hosseinpour, I. (2022). Ground improvement techniques applied to very soft clays: state of knowledge and recent advances. *Soil* *and Rocks*, 46(1), e2023008222. http://doi.org/10.28927/SR.2023.008222.

ASME BTH-1. (2008). *Design of below-the-hook lifting devices*. ASME - American Society of Mechanical Engineers, New York, USA.

ASTM E-23. (2018). *Notched Bar Impact Testing of Metallic Materials*. ASTM - American Society for Testing and Materials, Pennsylvania, USA.

ASTM E-18. (2019). *Standard test methods for rockwell hardness of metallic materials*. ASTM - American Society for Testing and Materials, Pennsylvania, USA.

Chen, W.F., & Han, D.J. (1988). *Plasticity for structural engineers*. New York: Springer.

Chen, W.F., & Zhang, H. (1991). *Structural plasticity: theory, problems and CAE software*. New York: Springer.

Craig, R.F. (2012). *Mecânica dos solos.* Rio de Janeiro: LTC (in Portuguese).

Feng, S.J., Shui, W.H., Tan, K., Gao, L.Y., & He, L.H. (2011). Field Evaluation of Dynamic Compaction on granular deposits. *Journal of Performance of Constructed Facilities*, 25(3), 241-249. http://doi.org/10.1061/(ASCE)CF.1943-5509.0000160.

Feng, S.J., Tan, K., & Shui, W.H. (2015). Dynamic Compaction of ultra-high energy in combation with ground replacement in coastal reclamation area marine. *Marine Georesources and Geotechnology*, 33(2), 109-121. http://doi.org/10.1080/1064119X.2013.805288.

Gambin, M.P. (1983). The menard dynamic consolidation at nice airport. In *Proceedings of the 8th European Conference on Soil Mechanics and Foundation Engineering* (pp. 231-234). Helsinki.

Ghassemi, A., Pak, A., & Shahir, H. (2009). Validity of Menard Relation in dynamic compaction operations. *Ground Improvement*, 162(1), 37-45. http://doi.org/10.1680/grim.2009.162.1.37.

Giese, D.N. (2019). *Compactação dinâmica em solo coesivo friccional* [Master's dissertation]. Federal University of Rio Grande do Sul (in Portuguese).

Hajialilue-Bonab, M., & Rezaei, A.H. (2009). Physical modelling of low-energy dynamic compaction international. *Journal of Physical Modelling in Geotechnics*, 9(3), 21-32. http://doi.org/10.1680/ijpmg.2009.090302.

Hamidi, B. (2014). *Distinguished ground improvement projects by dynamic compaction of dynamic replacement* [Doctoral thesis, Curtin University]. Curtin University's repository. Retrieved in November 27, 2024, from http://hdl.handle.net/20.500.11937/66

Han, J. (2015). *Principles and practice of ground improvement.* New York: John Wiley & Sons.

Ingles, O.G., & Metcalf, J.B. (1973). *Soil stabilization: principles and practice*. New York: John Wiley & Sons.

Kézdi, A. (1979). *Stabilized earth roads*. Amsterdam: Elsevier.

Koerner, R.M. (1997). *Designing with geosynthetics*. Pearson.

Lukas, R.G. (1995). *Dynamic compaction* (Geotechnical Engineering Circular, No. 1). National Technical Information Service.

Mayne, P.W., Jones Jr, J.S., & Dumas, J.Y. (1984). Ground response to dynamic consolidation. *Journal of Geotechnical Engineering*, 110(6), 757-774. http://doi.org/10.1061/(ASCE)0733-9410(1984)110:6(757).

Mehdipour, S., & Hamidi, A. (2017). Impact of tamper shape on the efficiency and vibrations induced during dynamic compaction of dry sands by 3D finite element modelling. *Civil Engineering Infrastructures Journal*, 50(1), 151-163. http://doi.org/10.7508/ceij.2017.01.009.

Menard, L. (1974). La consolidation Dynamique des sols de fondation. *Annales de l'ITBTP*, *320*, 194-220.

Menard, L., & Broise, Y. (1975). Theoretical and practical aspects of dynamic consolidation. *Geotechnique*, 25(1), 3-17. http://doi.org/10.1680/geot.1975.25.1.3.

Mitchell, J. (1981). Soil improvement: state of art. In *Proceedings of the 10th International Conference on Soil Mechanics and Foundation Engineering* (pp. 509-585). Stockholm.

Oshima, A., & Takada, N. (1997). Relationship between compacted area and ram momentum by heavy tamping. In *Proceedings of the International Conference Soil mechanics foundation engineering* (Vol. 3, pp. 1641-1644). Hamburg.

Pan, J.L., & Selby, A.R. (2002). Simulation of dynamic compaction of loose granular soils. *Advances in Engineering Software*, 33(7), 631-640. http://doi.org/10.1016/S0965-9978(02)00067-4.

Porán, C.J., & Rodriguez, J.A. (1992). Design of dynamic compaction. *Canadian Geotechnical Journal*, 29(5), 796-802. http://doi.org/10.1139/t92-087.

Rizzon, M.M. (2016). *Efeito da compactação dinâmica em solo residual* [Master's dissertation, Federal University of Rio Grande do Sul]. Federal University of Rio Grande do Sul`s repositor (in Portuguese). Retrieved in November 27, 2024, from http://hdl.handle.net/10183/149803.

Rollins, K.M., & Rogers, G.W. (1994). Mitigation measures for small structures on collapsible alluvial soils. *Journal of Geotechnical Engineering*, 120(9), 1533-1553. http://doi.org/10.1061/(ASCE)0733-9410(1994)120:9(1533).

Slocombe, B.C. (2013). Dynamic compaction. In K. Kirsch & A. Bell (Eds.), *Ground improvement* (pp. 57-86). Chapman & Hall.

Smits, M.T.J.H., & De Quelerij, L. (1989). The effect of dynamic compaction on dry granular soils. In *Proceedings of the 12th International Conference on Soil Mechanics and Foundations Engineering* (Vol. 2, pp. 1419-1422). Rio de Janeiro.

Souza Júnior, T.F.D. (2021). *Dynamic replacement method applied in clay laterític soil* [Doctoral thesis, Federal University of Rio Grande do Sul]. Federal University of Rio Grande do Sul`s repository. Retrieved in November 27, 2024, from http://hdl.handle.net/10183/236122

Tarawneh, B., Bodour, W., Shatnawi, A., Ajmi, K.A. (2019). Field evaluation and behavior of the soil improved using dynamic replacement. *Case Studies in Construction Materials*, *10*, 1-11. http://doi.org/10.1016/j.cscm.2018.e00214.

Tarawneh, B., Sbitnev, A., & Hakam, Y. (2017). Lessons learned from 11 million m^2 of dynamic compaction and replacement. *Proceedings of the Institution of Civil Engineers - Ground Improvement*, 170(4), 208-217. http://doi.org/10.1680/jgrim.17.00025.

Terashi, M., & Juran, I. (2000). Ground improvement: state of the art. In *Proceedings of the ISRM International Symposium* (pp. 461-519). Melbourne.